ACS APPLIED MATERIALS & INTERFACES

Research Article

www.acsami.org

Robust Multilayered Encapsulation for High-Performance Triboelectric Nanogenerator in Harsh Environment

Qiang Zheng,[†] Yiming Jin,[†] Zhuo Liu,[‡] Han Ouyang,[†] Hu Li,[‡] Bojing Shi,[†] Wen Jiang,[†] Hao Zhang,[#] Zhou Li,[*,†] and Zhong Lin Wang[†,∥]

[†]Beijing Institute of Nanoenergy and Nanosystems, National Center for Nanoscience and Technology (NCNST), Chinese Academy of Sciences, Beijing 100083, China

[‡]School of Biological Science and Medical Engineering, Beihang University, Beijing 100191, China

[#]Institute of Cardiothoracic Surgery at Changhai Hospital, Second Military Medical University, Shanghai 200433, China

[∥]School of Materials Science and Engineering, Georgia Institute of Technology, Atlanta, Georgia 30332-0245, United States

Supporting Information

ABSTRACT: Harvesting biomechanical energy especially *in vivo* is of special significance for sustainable powering of wearable/implantable electronics. The triboelectric nanogenerator (TENG) is one of the most promising solutions considering its high efficiency, low cost, light weight, and easy fabrication, but its performance will be greatly affected if there is moisture or liquid leaked into the device when applied *in vivo*. Here, we demonstrate a multiple encapsulation process of the TENG to maintain its output performance in various harsh environments. Through systematic studies, the encapsulated TENG showed great reliability in humid or even harsh environment over 30 days with a stability index of more than 95%. Given its outstanding reliability, the TENG has the potential to be applied in variety of circumstances to function as a sustainable power source for self-powered biomedical electronics and environmental sensing systems.

KEYWORDS: *biomechanical energy harvesting, self-powered biomedical electronics, multilayered encapsulation, flexible, triboelectric nanogenerator, reliability in harsh environment, waterproofness, corrosion resistance*

INTRODUCTION

In the past decades, huge efforts have been devoted to develop new-type alternative energy scavenging devices due to the ever-increasing energy crisis. The scavenging of energy from the environment is an ideal solution for sustainably powering the electronic systems. Several methods to harvest energy from chemical, mechanical, electrical, thermal, and photovoltaic processes have been demonstrated, such as using glucose oxidation, human motion, flow caused vibration, radio frequency, temperature gradient, and sun radiation,[1−5] among which mechanical energy harvesting has attracted much attention for its wide distribution and abundance. Previous existing approaches have been successfully demonstrated to convert mechanical energy into electricity by electromagnetism[6−8] and piezoelectricity.[9−15] Recently, a new type of mechanical-to-electrical energy conversion device termed the triboelectric nanogenerator (TENG) which is based on the coupling of contact electrification and electrostatic induction has been demonstrated.[16−20] Considering its high efficiency, low cost, light weight, and easy fabrication, the TENG can be as one of the most promising devices to harvest mechanical energy from environment such as body motion, wind, and ocean waves.[21−26] In addition, the TENG can also be implanted *in vivo* as a lifetime power source to drive medical devices such as pacemaker and sensing systems.[27−29] However, the output performance of the TENG is dramatically affected by factors, especially humidity.[30,31] Thus, it is of great significance and urgency to develop an complete encapsulation process to realize high performance TENG under a wide range of harsh environments.

Package layers are important to the TENG in two aspects. For one thing, good package layers will protect the components of the TENG and impede the corrosion from outside surroundings, thus contributing to a steady performance; for another thing, the potential leaking risk of materials inside the TENG can be eliminated, which is especially important when implanted *in vivo*.

Here, we demonstrate a newly designed flexible multilayered encapsulation structure for protecting the TENG from surrounding humid or even harsh environment. The encapsulated TENG showed outstanding reliability in various working conditions, which was crucial for mechanical energy harvesting.

Received: June 11, 2016
Accepted: September 22, 2016
Published: September 22, 2016

Downloaded via BEIJING INST NANOENERGY NANOSYSTEMS on January 3, 2020 at 03:28:42 (UTC).
See https://pubs.acs.org/sharingguidelines for options on how to legitimately share published articles.

© 2016 American Chemical Society

DOI: 10.1021/acsami.6b06866
ACS Appl. Mater. Interfaces 2016, 8, 26697−26703

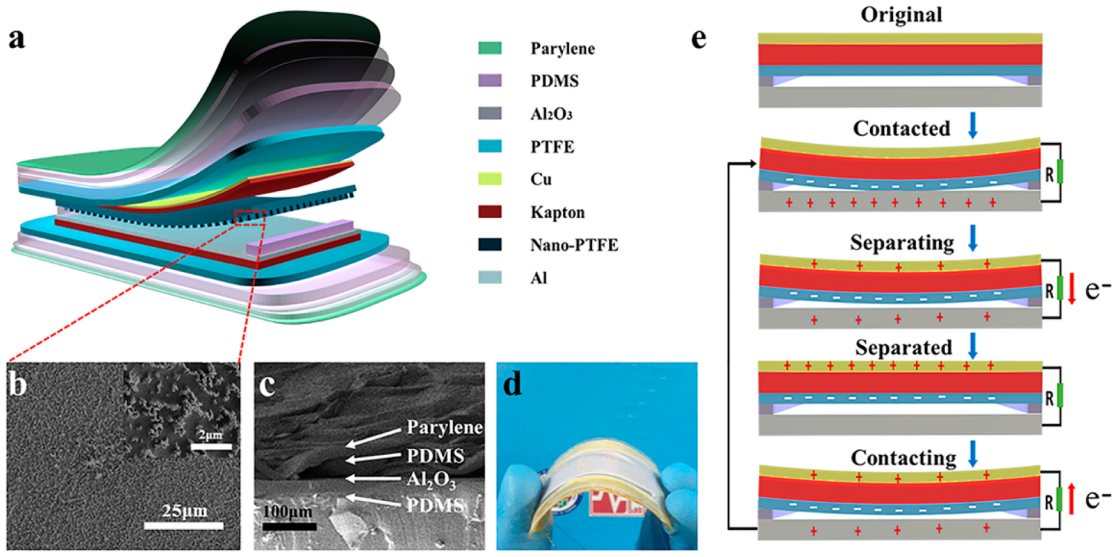

Figure 1. Structure design and working principle of the TENG. (a) 3D explosion view of the TENG. (b) SEM image of the nanostructured PTFE film; the scale bar is 25 μm. Inset is a magnified view with a scale bar of 2 μm. (c) Cross-sectional SEM image of the encapsulation layers of the TENG; the scale bar is 100 μm. (d) Photograph of the bent TENG demonstrating its good flexibility. (e) 3D schematic illustration of the working principle of the TENG.

Systematic stability studies of the TENG in humid and harsh environments were first carried out, which showed that the as fabricated TENG could survive in solutions with high osmotic pressure, strong ionic strength, acidity, and alkalinity for over 30 days without sacrificing too much of its output performance. In addition, the device can also maintain stable performance after suffering continuous temperature changes and mechanical impact of millions working cycles. This work may not only pave a road for the TENG as a sustainable power source for medical devices but also promote the future development of self-powered biomedical electronics and environmental sensing systems.

EXPERIMENTAL SECTION

Fabrication of the Nude TENG and the TENG. The as-fabricated nude TENG is of classical vertical contact-separation mode. Nanostructured PTFE and rough Al sheet were employed as triboelectric layers. The nano-PTFE was formed by inductively coupled plasma (ICP) with the etching gas of Ar, O_2, and CF_4. The nano-PTFE film was adhered to a Kapton substrate, and Cu film (100 nm) was deposited on the Kapton by magnetron sputter as electrode. Two package groups were involved in the encapsulation process of nude TENG: the first package group is PTFE/PDMS/Al_2O_3 composite layers, and the second package group is PDMS/parylene composite layers. Commercial PTFE was used without further treatment. Then PDMS mixed with specific ratio of curing agent were spin-coated on the device as the second package layer. After solidifying in 80 °C for an hour, Al_2O_3 film (40 nm) was also deposited by atomic layer deposition (ALD). Another thin layer of PDMS solution and 5 μm parylene film were further applied in sequence.

Cell Culture. The L929 cells were purchased from Central South University (Hunan, CHN). The cells were cultured in a 75 cm^2 flask with RPMI medium 1640 basic (1×), supplemented with 10% FBS (Gibco) and 1% penicillin−streptomycin solution (Life Technologies, Shanghai, CHN) at 37 °C in a humidified atmosphere with 5% CO_2.

Cell Viability. After being cultured for 3 days, L929 cells were seeded in culture plates with a density of 10^4 cells/well. In the experiment group, cells were cultured on encapsulation materials while cells were cultured on plates in the control group. Trypan blue staining showed that 98.5% of L929 cells were positive. The proliferation of the cultured L929 cells was determined using the MTT (3-{4,5-dimethylthiazol-2yl}-2,5-diphenyl-2*H*-tetrazolium bromide) assay. First, MTT solution (20 μL) was added to each well. Upon incubation at 37 °C for 4 h in a humidified atmosphere with 5% CO_2, MTT was taken up by active cells and reduced in the mitochondria to insoluble purple formazan granules. Subsequently, the medium was discarded, the precipitated formazan was dissolved in DMSO (100 μL/well), and then the optical density of the solution was evaluated using a microplate spectrophotometer at a wavelength of 490 nm. The analytical assays were performed at day 1, day 2, and day 3. At least four wells were randomly examined each time.

Cell Morphology and Immunofluorescent Staining. The cytoskeletal and nucleus were stained with Phalloidin and DAPI, respectively. In detail, the samples were fixed with immunohistochemically fixed fluid (Beyotime) for 30 min and then rinsed three times with prewarmed PBS. The samples were blocked with 0.1% BSA solution for 1 h at 37 °C and then incubated with DAPI (1:400 diluted) and Alexa Fluor Phalloidin 568 conjugate (1:200 diluted) for 2 h at 37 °C.

Characterization Methods. The open-circuit voltage was measured by Tektronix oscilloscope, the short-circuit current, and transferred charge were measured using a Keithley 6514 system electrometer. The fabricated nanostructured PTFE film was processed by ALD system (Picosun Sunale R-200). The Cu electrode was deposited by magnetron sputter (Denton Discovery 635) and the parylene layer was deposited by the parylene coating system (PDS-2010 Labcoter2). The fluorescence photos of stained cells were imaged using an inversion fluorescence microscope (Olympus IX71). All SEM images were taken by Hitachi field emission scanning electron microscope (SU 8020). All AFM images were taken by Asylum Research MFP-3D-SA-DV.

RESULTS AND DISCUSSION

Figure 1a presents the flexible and multilayered structure of the fabricated TENG (60 mm × 40 mm × 1.5 mm) which was composed of the nude TENG (45 mm × 25 mm × 0.9 mm) and encapsulation structure. The nude TENG mainly consisted of three components: electrodes, triboelectric layers, and spacers. Polytetrafluoroethylene (PTFE) film (25 μm) with surface nanostructures (nano-PTFE) prepared by inductively coupled plasma (ICP) etching was adopted as one of the triboelectric layers to increase the output electrical signals

DOI: 10.1021/acsami.6b06866
ACS Appl. Mater. Interfaces 2016, 8, 26697−26703

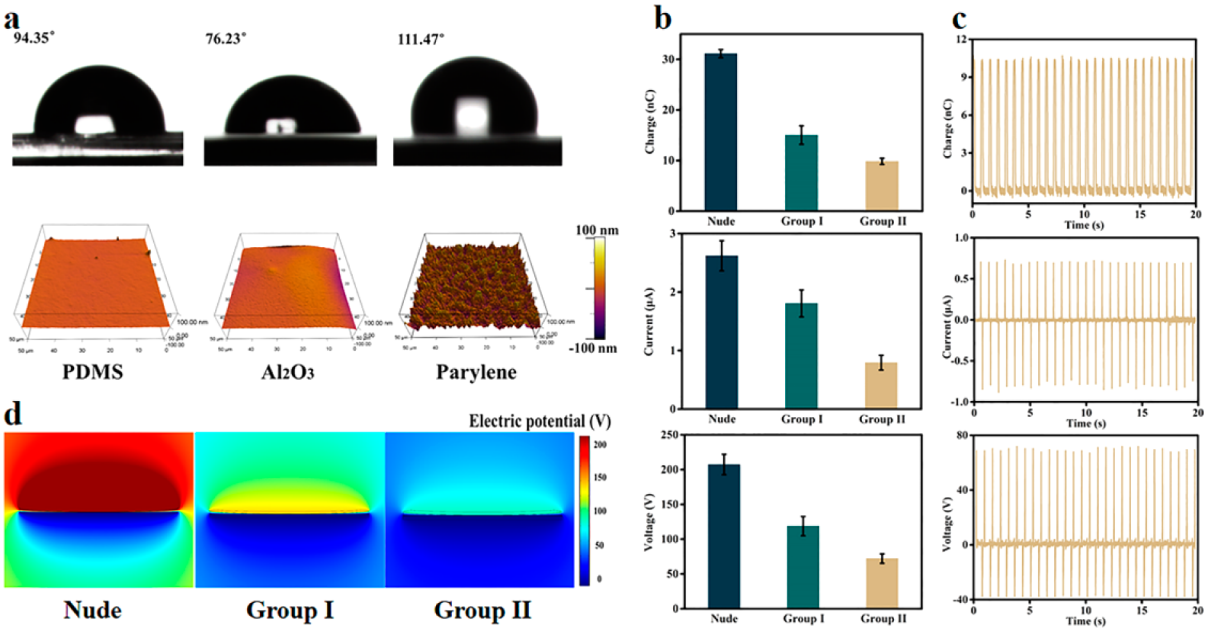

Figure 2. Characterization and output performance of the TENG in different encapsulation stages. (a) Contact angle data and AFM images of the PDMS, Al_2O_3, and parylene film. (b) Statistical graph of the output electrical signals of the TENG in different package status. The measured signals include open-circuit voltage, short-circuit current, and transferred charge. The package group I is PTFE/PDMS/Al_2O_3 composite layers, and the package group II is PDMS/parylene composite layers. (c) Detailed waveforms of the transferred charge, short-circuit current, and open-circuit voltage of the as-fabricated TENG. (d) Cross-sectional view of the numerical simulation results of electric potential distribution for the TENG in different package process via COMSOL.

(Figure 1b). The nano-PTFE film was adhered to a Kapton substrate (100 μm), and Cu film (100 nm) was deposited on the back side of the Kapton by magnetron sputter as one electrode. A rough Al sheet (90 μm) was employed as both another triboelectric layer and electrode which was integrated with a Kapton substrate (220 μm) to increase its flexibility and strength. The spacer layer (500 μm, PDMS) was placed between two triboelectric layers to further guarantee the effective contact and separation process.

The key feature of the encapsulated TENG layout was that the nude TENG resided in a flexible and laminated structure which provided isolation from surroundings. Materials with outstanding biocompatibility and stability were chosen for the encapsulation of the TENG. PTFE (60 μm) was used as the first package layer for its good biocompatibility and mechanical strength,[32] which also functioned as a substrate for further package layers. Polydimethylsiloxane (PDMS) mixed with specific ratio of curing agent were then spin-coated on the device for its great flexibility and hydrophobicity. This relative thick PDMS layer (170 μm) provided the device with waterproof capability and structural stability under external force and implanted environment. Al_2O_3 was then deposited onto the PDMS layer by atomic layer deposition (ALD) forming a dense metal oxide protective layer (40 nm) to fill the gap between polymer chains of PDMS, which significantly improved the waterproofness and anticorrosion performance of the TENG.[33−35]

The above-mentioned layers can be categorized as the first package group (Group I) because they endowed the TENG with good water-resisting ability. In order to reduce erosion in physiological or harsh environment while maintain high steadiness, the second package group was further applied (Group II). Parylene-C (5 μm) was deposited by the parylene coating system to form high density and hole-free coating layer which is waterproof and anticorrosive.[36,37] In addition, to reduce the unnecessary weak adhesions between particle layers, a thin layer of PDMS (50 μm) was also added between Al_2O_3 and parylene. The cross-sectional scanning electron microscopy (SEM) image of the encapsulation layers is displayed showing the laminated structure (Figure 1c). A photograph of the bent TENG showed its great flexibility and deformation-recovery ability (Figure 1d). Even bended to a bending degree of 50%, the device could recover to its original state and maintain its function (Figure S6).

The detailed working principle based on the coupling of contact electrification and electrostatic induction of the TENG is illustrated in Figure 1e. Electrons are driven back and forth through the external circuit when compressed and released, thus contributing to cyclic alternating signals.

PDMS, Al_2O_3, and parylene were key components of the encapsulation layers which endowed the TENG with waterproofness and corrosion resistance. To prove the existence of the ultrathin Al_2O_3 and parylene film, water contact angle (WCA) and atomic force microscopy (AFM) tests were adopted. As shown in Figure 2a, the WCA reduced from 94° to 76° after the deposition of Al_2O_3 and then increased to 111° after the parylene coating process. This phenomenon consisted with the intrinsical difference of hydrophobicity of those adopted encapsulation materials. AFM imaging further confirmed the flat and hole-free surface of the encapsulation layers, which was important for their waterproofness. Moreover, as the parylene deposited, surface structures in nanoscale was automatically formed, which contributed to its good hydrophobicity. The different surface morphologies and hydrophobic degrees demonstrated the successful encapsulation of the different layers of PDMS, Al_2O_3, and parylene.

The effect of the encapsulation process on the TENG output performance was studied systematically. As illustrated pre-

DOI: 10.1021/acsami.6b06866
ACS Appl. Mater. Interfaces 2016, 8, 26697−26703

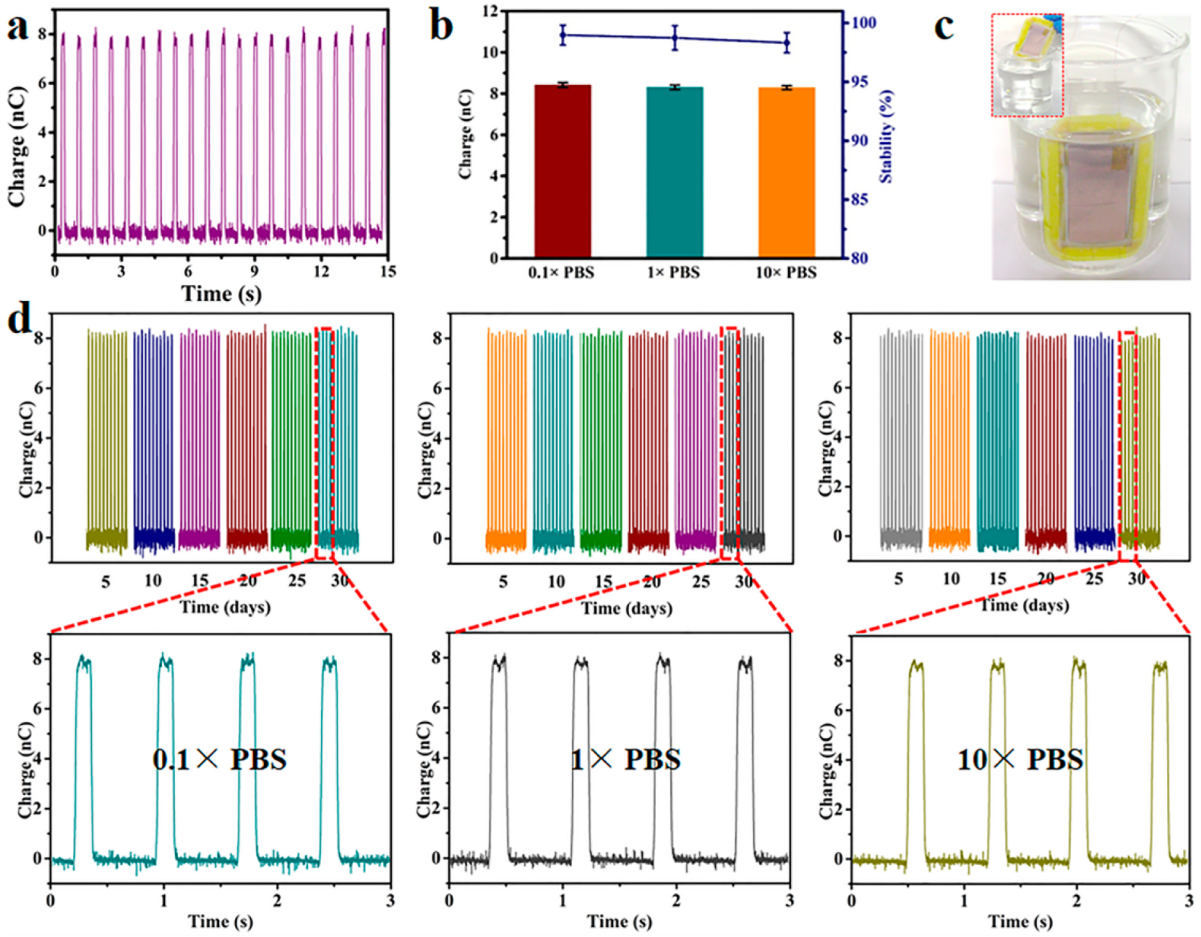

Figure 3. Transferred charge of the TENG with and without PBS treatment. (a) Transferred charge of the as-fabricated TENG without PBS treatment. (b) Statistical chart of the transferred charge of the TENG applied in different PBS solution and its stability index. (c) Photograph of the TENG applied in PBS solution. (d) Measured transferred charge of the TENG after immersing in 0.1×, 1×, and 10× PBS solution and its corresponding detailed waveforms after immersing for 30 days. The measurement were taken every 24 h.

viously,[38,39] the open-circuit voltage and capacitance of the TENG in vertical contact-separation mode can be described by the following equations:

$$V_{\mathrm{TENG}} = \frac{\sigma x}{\varepsilon_0} \tag{1}$$

$$C_{\mathrm{TENG}} = \frac{\varepsilon_0 S}{d_0 + x} \tag{2}$$

where ε_0 is the permittivity in vacuum, σ is the triboelectric charge density, x is the vertical gap distance between the two triboelectric layers, d_0 is the effective dielectric thickness, and S is the area of dielectric layer. The value of triboelectric charge density σ depends on the triboelectric materials and their contact areas which can be considered as constant in this work.

Based on the theoretical equations, it can be easily anticipated that the gap distance and dielectric thickness of the TENG will change accordingly in the encapsulation process, which in turn affected the output performance of the TENG. Therefore, the electrical output signals were measured as encapsulation proceeded. As we described above, two package groups were applied in the whole process; Group I contains PTFE, PDMS, and Al_2O_3, and Group II contains PDMS and parylene. Detailed values of the output signals in different stages are depicted in Figure 2b. All of the output signals experienced a decline as the package process goes on. The transferred charge, short-circuit current, and open-circuit voltage of the nude TENG were 31 nC, 2.6 μA, and 200 V, respectively. While after layer by layer encapsulation processes, the values still reached to 10.5 nC, 0.8 μA, and 70 V (Figure 2c). The output power of TENG after encapsulation can reach to 16 μW at the load resistance of 133 MΩ (Figure S7). To understand the mechanism of the reduction of TENG output associated with encapsulation process, the electric potential distribution in the device was simulated using COMSOL. The model proposed based on the real dimensions of TENG. The Al_2O_3 (40 nm) and parylene (5 μm) layers were not involved in this model because they are ultrathin film comparing to the entire thickness of whole device (1 mm) and can hardly affect the mechanical properties of TENG. The simulated open-circuit voltage of the TENG at different encapsulation stage was 277, 133, and 87.3 V, respectively, which were consistent with the experimentally measured data. The finite element method (FEM) results of the electric potential distribution for the TENG in different package process via COMSOL indicate that the electric potential of triboelectric layers indeed decline as the encapsulation process carry on (Figure 2d).

Through the theoretical simulation, the reduction in electrical outputs can be ascribed to the increasing load burden of elastic Kapton substrate as encapsulation layers continuously

DOI: 10.1021/acsami.6b06866
ACS Appl. Mater. Interfaces 2016, 8, 26697−26703

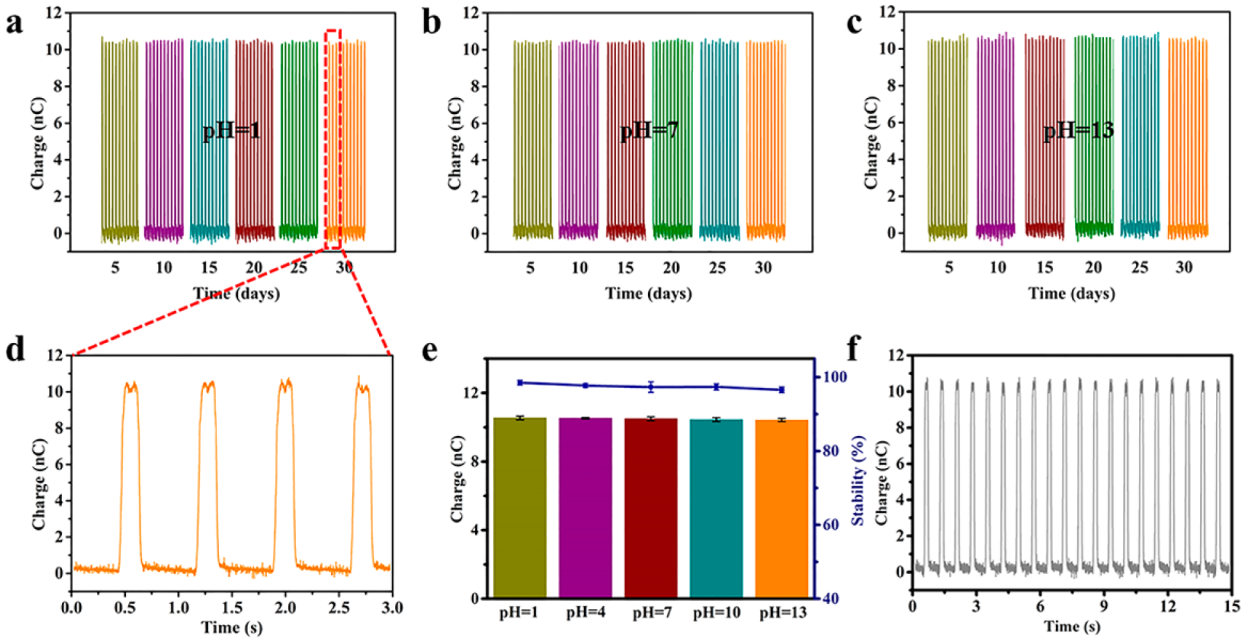

Figure 4. Stability test of the TENG against solution with different pH values. (a–c) Measured amount of transferred charge of the TENG after immersing in pH = 1, 7, and 13 solution, respectively. The measurements were taken every 24 h. (d) Detailed transferred charge waveforms of the TENG after immersing in pH = 1 solution for 30 days. (e) Statistical chart of the transferred charge of the TENG applied in solution with different pH values and its stability index. (f) Transferred charge of the as-fabricated TENG without acid or alkali solution treatment.

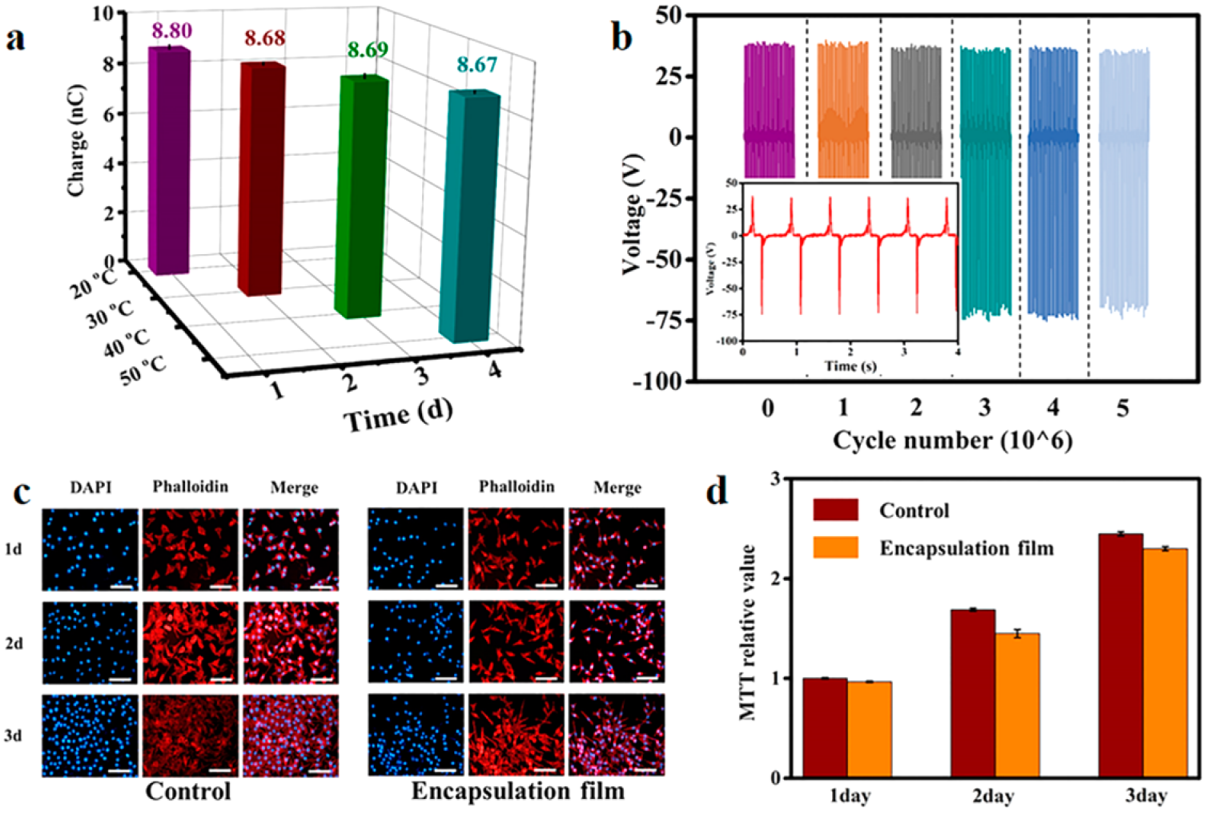

Figure 5. Thermally, mechanically, and biologically characterization of the TENG. (a) Transferred charge of the TENG in solution with different temperature. (b) Open-circuit voltage of the TENG and its durability test with a magnified view of the waveform in the inset. (c) Fluorescence images of stained L929 cells that were cultured on encapsulation layers of the TENG; the scale bar is 100 μm. (d) Cell viability after being cultured for 1, 2, and 3 days. MTT results show that viability of L929 cells was not seriously affected by the encapsulation layers of the TENG.

piled on. The weakening of reversibility and elasticity resulted in a smaller space between the two triboelectric layers and thicker dielectric layers. According to eqs 1 and 2, reduced gap distance and elevated dielectric thickness will lower the output performance of the TENG. Moreover, in our experiment, the existence of the gap between two friction layers will leave some

DOI: 10.1021/acsami.6b06866
ACS Appl. Mater. Interfaces 2016, 8, 26697–26703

air inside the encapsulated device. The residual air has chances to affect the output performance of our encapsulated device by partially offsetting the external force and increasing the resistance of the contact process.

TENG is one of the most promising devices that can harvest mechanical energy from surroundings, but its performance will be greatly affected by humid environmental conditions especially when applied *in vivo*. To prove the reliability of applying the TENG in humid atmosphere with different osmotic pressures as well as the potential for resisting the accelerated aging caused by the ionic strength *in vivo*, it was applied in different concentrations of phosphate buffered saline (PBS) solution (0.1×, 1×, and 10×), and its electrical outputs were recorded.

Before treated with PBS solution, the transferred charge of the TENG was measured as initial state which is shown in Figure 3a. Then, the TENG was applied in PBS solution with different concentrations, and the transferred charge was measured every 24 h (Figure 3b,c). It can be seen clearly that even after immersed in 10× PBS solution for over 30 days, the amount of transferred charge was still stable and remained at around 8 nC, showing the good resistance of the TENG to water and strong ionic strength. The corresponding short-circuit current was also stable over the 30 days test (Figure S1). As described in previous literature on accelerated PBS etching test,[30] the survival of the TENG in 10× PBS for over 30 days can be as an accelerated test which projected to an improved chemical stability in the normal physiological condition for over 300 days. Statistical analysis of the transferred charge of the TENG applied in different PBS solution further proved the above conclusion. The stability index was an indicator obtained by the ratio between the outputs of the TENG after and before treatment which was defined to evaluate its performance in harsh environment. It can be inferred from Figure 3b that after experiencing a series of PBS treatment, the stability index of the TENG is still over 98% compared to the original one. This demonstrates the reliability of the TENG in humid atmosphere and the potential for working in physiological conditions.

To test the anticorrosion performance of the TENG and display the possibility of applying it in harsh environment especially in strong acid and strong alkali conditions, the TENG was applied in solution with different pH values. The pH value gradient we adopted here was pH = 1, 4, 7, 10, and 13 adjusted by NaOH and HCl. All acidic solution and alkaline solution were contained in Teflon beakers and sealed to avoid unnecessary moisture absorption and evaporation.

The TENG was immersed in solution with different pH values mentioned above; the transferred charges and short-curcuit current were measured respectively every 24 h (Figure 4a–e, Figures S2 and S3). Figure 4d shows the detailed transferred charge waveforms of the TENG after immersing in pH = 1 solution for 30 days, and Figure 4f shows the transferred charge of the as-fabricated TENG without interaction with acid or alkali solution. The statistical analysis chart showed that after immersing in pH = 1, 4, 7, 10, and 13 solution for 30 days, the amount of transferred charge was still stable and remained at around 10.5 nC (Figure 4e). The stability index value of the TENG defined previously was higher than 95% and also showed its great corrosion-resisting property.

The TENG was immersed in solution with different temperatures in succession; the temperature gradient was set 10 °C per day. It can be seen from the measured transferred charge (Figure 5a) that the TENG can endure the thermal stress in the range of 20–50 °C, which was sufficient for the TENG to be implanted *in vivo*. In addition, results from the penetration test showed that the TENG can survive in 80 °C red dye solution for 2 h without any leakage (Figure S4). Figure 5b shows the long-term performance of the TENG against external mechanical force applied by linear motor. Even after 5 million working cycles, the open-circuit voltage of the TENG maintained stable compared with its initial state (V_{oc} = 70 V) exhibiting its outstanding durability.

Cell MTT assay was also designed to evaluate the biocompatibility of the TENG. Mouse fibroblast (L929) was adopted for the cytotoxicity analysis. L929 cells were seeded on the encapsulation layers of the TENG and cell culture dish; their adherence, spreading, and viability were analyzed. The fluorescence images and SEM image of stained cells showed explicitly that they adhered to both substrates well with evident spreading and intact cytoarchitecture (Figure 5c and Figure S5). The MTT value of the experiment group was similar to the value of the control group after 3 days of culture. These results mentioned above not only demonstrated the good cytocompatibility of the TENG but also revealed the leak-free ability of the encapsulation layers. Therefore, concerns on the potential risk of hazardous materials inside the TENG such as metal nanoparticles can be relieved.

CONCLUSION

In summary, we have demonstrated a multiple encapsulation process of the TENG to overcome obstacles when applied in humid environments. The flexible laminated encapsulation structures endow the TENG with good waterproofness and corrosion resistance, allowing its stable output performance in harsh environment for over 30 days. It has been demonstrated that the TENG has outstanding reliability in chemically, physiologically, thermally, and mechanically harsh environment. This will provide a promising power source for self-powered biomedical electronics and environmental sensing systems.

ASSOCIATED CONTENT

Supporting Information

The Supporting Information is available free of charge on the ACS Publications website at DOI: 10.1021/acsami.6b06866.

More detailed data, images, and movies about the cytocompatibility, output current, red ink tests, flexibility tests, and load matching tests (PDF)

AUTHOR INFORMATION

Corresponding Author

*E-mail: zli@binn.cas.cn (Z.L.).

Author Contributions

Q.Z., Y.J., and Z.L. contributed equally to this work.

Notes

The authors declare no competing financial interest.

ACKNOWLEDGMENTS

This work was supported by the national key R & D project from Minister of Science and Technology, China (2016YFA0202703), NSFC (31571006), Beijing Talents Fun (2015000021223ZK21) and "Thousands Talents" program for pioneer researcher and his innovation team. The authors want

DOI: 10.1021/acsami.6b06866
ACS Appl. Mater. Interfaces 2016, 8, 26697–26703

to thank Prof. Dan Peng for her contribution of discussing the materials fabrication and stability tests in this work.

REFERENCES

(1) Cosnier, S.; Le Goff, A.; Holzinger, M. Towards Glucose Biofuel Cells Implanted in Human Body for Powering Artificial Organs: Review. *Electrochem. Commun.* **2014**, *38*, 19−23.
(2) Wang, D. A.; Ko, H. H. Piezoelectric Energy Harvesting from Flow-induced Vibration. *J. Micromech. Microeng.* **2010**, *20*, 025019.
(3) Le, T.; Mayaram, K.; Fiez, T. Efficient Far-field Radio Frequency Energy Harvesting for Passively Powered Sensor Networks. *IEEE J. Solid-State Circuits* **2008**, *43*, 1287−1302.
(4) Ujihara, M.; Carman, G. P.; Lee, D. G. Thermal Energy Harvesting Device Using Ferromagnetic Materials. *Appl. Phys. Lett.* **2007**, *91*, 093508.
(5) Garnett, E. C.; Yang, P. D. Silicon Nanowire Radial p-n Junction Solar Cells. *J. Am. Chem. Soc.* **2008**, *130*, 9224−9225.
(6) Rome, L. C.; Flynn, L.; Goldman, E. M.; Yoo, T. D. Generating Electricity while Walking with Loads. *Science* **2005**, *309*, 1725−1728.
(7) Donelan, J. M.; Li, Q.; Naing, V.; Hoffer, J. A.; Weber, D. J.; Kuo, A. D. Biomechanical Energy Harvesting: Generating Electricity During Walking with Minimal User Effort. *Science* **2008**, *319*, 807−810.
(8) Dai, D.; Liu, J. Hip-mounted Electromagnetic Generator to Harvest Energy from Human Motion. *Front. Energy.* **2014**, *8*, 173−181.
(9) Jung, W. S.; Lee, M. J.; Kang, M. G.; Moon, H. G.; Yoon, S. J.; Baek, S. H.; Kang, C. Y. Powerful Curved Piezoelectric Generator for Wearable Applications. *Nano Energy* **2015**, *13*, 174−181.
(10) Chun, J.; Kang, N. R.; Kim, J. Y.; Noh, M. S.; Kang, C. Y.; Choi, D.; Kim, S. W. Highly Anisotropic Power Generation in Piezoelectric Hemispheres Composed Stretchable Composite Film for Self-powered Motion Sensor. *Nano Energy* **2015**, *11*, 1−10.
(11) Shenck, N. S.; Paradiso, J. A. Energy Scavenging with Shoe-Mounted Piezoelectrics. *IEEE Micro.* **2001**, *21*, 30−42.
(12) Shin, S. H.; Kim, Y. H.; Lee, M. H.; Jung, J. Y.; Nah, J. Hemispherically Aggregated $BaTiO_3$ Nanoparticle Composite Thin Film for High-performance Flexible Piezoelectric Nanogenerator. *ACS Nano* **2014**, *8*, 2766−2773.
(13) Cha, S. N.; Seo, J. S.; Kim, S. M.; Kim, H. J.; Park, Y. J.; Kim, S. W.; Kim, J. M. Sound-Driven Piezoelectric Nanowire-Based Nanogenerators. *Adv. Mater.* **2010**, *22*, 4726−4730.
(14) Jeong, C. K.; Lee, J.; Han, S.; Ryu, J.; Hwang, G.-T.; Park, D. Y.; Park, J. H.; Lee, S. S.; Byun, M.; Ko, S. H.; Lee, K. J. A Hyper-Stretchable Elastic-Composite Energy Harvester. *Adv. Mater.* **2015**, *27*, 2866−2875.
(15) Jeong, C. K.; Park, K.-I.; Son, J. H.; Hwang, G.-T.; Lee, H. L.; Park, D. Y.; Lee, H. E.; Lee, H. K.; Byun, M.; Lee, K. J. Self-Powered Fully-Flexible Light-Emitting System Enabled by Flexible Energy Harvester. *Energy Environ. Sci.* **2014**, *7*, 4035−4043.
(16) Fan, F. R.; Tian, Z. Q.; Wang, Z. L. Flexible Triboelectric Generator. *Nano Energy* **2012**, *1*, 328−334.
(17) Zhu, G.; Lin, Z. H.; Jing, Q. S.; Bai, P.; Pan, C. F.; Yang, Y.; Zhou, Y. S.; Wang, Z. L. Toward Large-scale Energy Harvesting by a Nanoparticle-enhanced Triboelectric Nanogenerator. *Nano Lett.* **2013**, *13*, 847−853.
(18) Wang, S. H.; Lin, L.; Wang, Z. L. Nanoscale Triboelectric-effect-enabled Energy Conversion for Sustainably Powering Portable Electronics. *Nano Lett.* **2012**, *12*, 6339−6346.
(19) Zhu, G.; Chen, J.; Liu, Y.; Bai, P.; Zhou, Y. S.; Jing, Q. S.; Pan, C. F.; Wang, Z. L. Linear-grating Triboelectric Generator Based on Sliding Electrification. *Nano Lett.* **2013**, *13*, 2282−2289.
(20) Lin, L.; Wang, S. H.; Xie, Y. N.; Jing, Q. S.; Niu, S. M.; Hu, Y. F.; Wang, Z. L. Segmentally Structured Disk Triboelectric Nanogenerator for Harvesting Rotational Mechanical Energy. *Nano Lett.* **2013**, *13*, 2916−2923.
(21) Zhang, H. L.; Yang, Y.; Hou, T. C.; Su, Y. J.; Hu, C. G.; Wang, Z. L. Triboelectric Nanogenerator Built Inside Clothes for Self-powered Glucose Biosensors. *Nano Energy* **2013**, *2*, 1019−1024.
(22) Yang, W. Q.; Chen, J.; Zhu, G.; Yang, J.; Bai, P.; Su, Y. J.; Jing, Q. S.; Cao, X.; Wang, Z. L. Harvesting Energy from the Natural Vibration of Human Walking. *ACS Nano* **2013**, *7*, 11317−11324.
(23) Quan, T.; Wang, X.; Wang, Z. L.; Yang, Y. Hybridized Electromagnetic-triboelectric Nanogenerator for a Self-Powered Electronic Watch. *ACS Nano* **2015**, *9*, 12301−12310.
(24) Zhao, Z. F.; Pu, X.; Du, C. H.; Li, L. X.; Jiang, C. Y.; Hu, W. G.; Wang, Z. L. Freestanding Flag-type Triboelectric Nanogenerator for Harvesting High-altitude Wind Energy from Arbitrary Directions. *ACS Nano* **2016**, *10*, 1780−1787.
(25) Wang, X. F.; Niu, S. M.; Yin, Y. J.; Yi, F.; You, Z.; Wang, Z. L. Triboelectric Nanogenerator Based on Fully Enclosed Rolling Spherical Structure for Harvesting Low-frequency Water Wave Energy. *Adv. Energy Mater.* **2015**, *5*, 1501467.
(26) Guo, H. Y.; Wen, Z.; Zi, Y. L.; Yeh, M. H.; Wang, J.; Zhu, L. P.; Hu, C. G.; Wang, Z. L. A Water-proof Triboelectric-electromagnetic Hybrid Generator for Energy Harvesting in Harsh Environments. *Adv. Energy Mater.* **2016**, *6*, 1501593.
(27) Zheng, Q.; Shi, B. J.; Fan, F. R.; Wang, X. X.; Yan, L.; Yuan, W. W.; Wang, S. H.; Liu, H.; Li, Z.; Wang, Z. L. In Vivo Powering of Pacemaker by Breathing-Driven Implanted Triboelectric Nanogenerator. *Adv. Mater.* **2014**, *26*, 5851−5856.
(28) Zheng, Q.; Zou, Y.; Zhang, Y.; Liu, Z.; Shi, B.; Wang, X.; Jin, Y.; Ouyang, H.; Li, Z.; Wang, Z. L. Biodegradable Triboelectric Nanogenerator as a Life-time Designed Implantable Power Source. *Sci. Adv.* **2016**, *2*, e1501478.
(29) Zheng, Q.; Zhang, H.; Shi, B. J.; Xue, X.; Liu, Z.; Jin, Y. M.; Ma, Y.; Zou, Y.; Wang, X. X.; An, Z.; Tang, W.; Zhang, W.; Yang, F.; Liu, Y.; Lang, X. L.; Xu, Z. Y.; Li, Z.; Wang, Z. L. In Vivo Self-Powered Wireless Cardiac Monitoring Via Implantable Triboelectric Nanogenerator. *ACS Nano* **2016**, *10*, 6510.
(30) Nguyen, V.; Yang, R. Effect of Humidity and Pressure on the Triboelectric Nanogenerator. *Nano Energy* **2013**, *2*, 604−608.
(31) Lee, K. Y.; Chun, J. S.; Lee, J. H.; Kim, K. N.; Kang, N. R.; Kim, J. Y.; Kim, M. H.; Shin, K. S.; Gupta, M. K.; Baik, J. M.; Kim, S. W. Hydrophobic Sponge Structure-based Triboelectric Nanogenerator. *Adv. Mater.* **2014**, *26*, 5037−5042.
(32) Pignatello, R. *Advances in Biomaterials Science and Biomedical Applications*; InTech: 2013.
(33) Zhou, W.; Dai, X.; Fu, T. M.; Xie, C.; Liu, J.; Lieber, C. M. Long Term Stability of Nanowire Nanoelectronics in Physiological Environments. *Nano Lett.* **2014**, *14*, 1614−1619.
(34) Hench, L. L. Bioceramics. *J. Am. Ceram. Soc.* **1998**, *81*, 1705−1728.
(35) Ratner, B. D.; Hoffman, A. S.; Schoen, F. J.; Lemons, J. E. *Biomaterials Science - An Introduction to Materials in Medicine*, 2nd ed.; Academic Press: New York, 2004.
(36) Fortin, J. B.; Lu, T. M. *Chemical Vapor Deposition Polymerization: The Growth and Properties of Parylene Thin Films*; Springer Science & Business Media: 2003.
(37) Tan, C. P.; Craighead, H. G. Surface Engineering and Patterning Using Parylene for Biological Applications. *Materials* **2010**, *3*, 1803−1832.
(38) Niu, S. M.; Zhou, Y. S.; Wang, S. H.; Liu, Y.; Lin, L.; Bando, Y.; Wang, Z. L. Simulation Method for Optimizing the Performance of an Integrated Triboelectric Nanogenerator Energy Harvesting System. *Nano Energy* **2014**, *8*, 150−156.
(39) Lin, L.; Xie, Y. N.; Wang, S. H.; Wu, W. Z.; Niu, S. M.; Wen, X. N.; Wang, Z. L. Triboelectric Active Sensor Array for Self-powered Static and Dynamic Pressure Detection and Tactile Imaging. *ACS Nano* **2013**, *7*, 8266−8274.

DOI: 10.1021/acsami.6b06866
ACS Appl. Mater. Interfaces 2016, 8, 26697−26703